

# Analyzing urban morphology changes using neural networks

*Sergiy Kostrikov*

DSc (Geography), Professor, K. Niemets Department of Human Geography and Regional Studies,

V. N. Karazin Kharkiv National University, Kharkiv, Ukraine,

e-mail: [sergiy.kostrikov@karazin.ua](mailto:sergiy.kostrikov@karazin.ua),  <https://orcid.org/0000-0002-4236-8474>

## ABSTRACT

**Introduction to the problem.** Urbanization demands advanced tools to analyze morphological changes caused by hostilities or disasters. This study bridges this gap by integrating artificial neural networks (ANNs) with LiDAR and GIS technologies, focusing on a site in Kharkiv, Ukraine, which was marginally impacted by the 2022 Russian invasion. Our key objective is to quantify urban resilience and transformation under extreme stress.

**Review of previous works.** Advances in CNNs and RNNs have enabled spatial-temporal analysis of LiDAR and multisource data. Recent methodologies improved feature extraction for urban change detection. However, gaps persisted in hostilities' zone analysis, airborne and terrestrial LiDAR integration, and interpretability of ANN-driven insights.

**Exposition of the main research material. Basics of ANNs for urban studies.** This study employs two custom architectures: 1. *ANN Similarity (Enhanced)*: A feedforward network using Mean Squared Error (MSE) loss and cosine similarity to predict dataset similarities. 2. *Latest ANN Method*: A deeper network with contrastive loss and Euclidean distance, emphasizing dissimilarity detection via convolutional/recurrent layers.

**Applications in urban studies.** The ANNs in this study were applied to the following from several listed industrial domains: 1. *Routine Urban Monitoring*: Detecting new constructions/demolitions in Tallinn, ESTONIA. 2. *Hostilities Impact Analysis*: Identifying war-induced structural changes in Kharkiv, UKRAINE. 3. *3D Feature Extraction*: Automating building volumetry and change detection mapping from LiDAR point clouds.

**Urban Remote Sensing with LiDAR.** LiDAR's millimeter-level accuracy enabled 3D modeling of urban features (e.g., building footprints, microtopography). Airborne (ALS) and mobile (MLS) LiDAR datasets were processed via proprietary *iQ City Change Management (CCM)* software, addressing challenges like ALS/MLS alignment and artifact filtering via point-density thresholds.

**Case Study: urban change detection using LiDAR to assess hostilities' impact. Methodology:** the study analyzed multitemporal LiDAR datasets: Kharkiv (2019–2022): a 4 km<sup>2</sup> zone in Northern Saltivka, devastated by shelling. Tallinn (2017–2022): control datasets for routine redevelopment.

**CCM Workflow:** 1. *Building Extraction (BE)*: identified structural features (Area, Volume, Height). 2. *Change Detection (CD)*: classified changes as *Added* (new construction), *Removed* (demolition), or *Unchanged*.

**ANN Analysis for comparing detected changes** through *Wolfram Mathematica*: compared ANSE (similarity-focused) and LANN (dissimilarity-driven) methods. **Results:** The following changes detected. Kharkiv: 215 *Added* (pre-war redevelopment) and 51 *Removed* (war-induced demolitions) changes. The LANN method revealed stark contrasts (score: 0.35 and 0.32-0.42) between war-driven vs. routine redevelopment demolitions, capturing irregular demolitions. Tallinn: predictable redevelopment patterns (scores: 0.60-0.66 and 0.74), validating ANN accuracy for routine changes. **Implications:** LANN's sensitivity to hidden features (e.g., structural degradation) gives policymakers detailed guidance for post-war recovery, and its divergence from statistical models highlights AI's power to reveal unseen urban dynamics.

**Conclusion.** This research demonstrates how ANNs, fused with LiDAR/GIS, transcend traditional urban monitoring limitations. The framework offers scalable tools for disaster recovery, particularly in war zones.

**Keywords:** LiDAR, urban studies, urban remote sensing, desktop software, building extraction, change detection, neural networks, analytical software, the first (ANSE) and the second (LANN) ANN analysis methods.

**In cites:** Kostrikov Sergiy (2025). Analyzing urban morphology changes using neural networks. Visnyk of V.N. Karazin Kharkiv National University. Series Geology. Geography. Ecology, (62), 219-236. <https://doi.org/10.26565/2410-7360-2025-62-17>

**Introduction to the problem.** Over the past several decades, the world has undergone a profound transition into an information-driven society, where urbanization has emerged as one of the most transformative forces of the 21st century. By 2050, nearly 70% of the global population is projected to reside in cities, a trend accompanied by unprecedented spatial, social, and environmental challenges [1]. Rapid urban expansion, coupled with dynamic morphological transformations - ranging from vertical densification to sprawling peri-urbanization - has necessitated advanced analytical frameworks capable of capturing and interpreting these changes with precision. In this context, geoinformation technologies, particularly

Geographic Information Systems (GIS) and Urban Remote Sensing (URS), have become indispensable. Tools such as LiDAR (Light Detection and Ranging) now provide millimeter-level accuracy in 3D urban mapping, enabling researchers to quantify structural changes in building heights, road networks, and green spaces with unprecedented fidelity [2]. Yet, as cities evolve into increasingly complex systems, traditional analytical methods struggle to decode the non-linear interactions between human activities, infrastructure, and ecological processes, that all define modern urban geosystems [3].

Our paper addresses this critical gap by integrating artificial intelligence (AI) in its artificial neural

network (ANN) presentation with geospatial technologies to redefine urban monitoring paradigms. The case is, that conventional approaches to urban change detection, rooted in 2D cartographic analysis and manual interpretation, often fail to account for the multidimensional nature of urban growth. For instance, methods relying on spectral indices or pixel-based classifications frequently overlook subtle morphological shifts, such as rooftop modifications or incremental land-use transitions, which are vital for understanding urban resilience [4]. Neural networks, however, offer a transformative alternative. By leveraging their capacity to discern intricate patterns within vast, heterogeneous datasets - from LiDAR point clouds to multi-temporal satellite imagery - these models excel at automating the detection of both abrupt and incremental urban changes, even in data-scarce environments.

Our research is anchored in the urbogeosystemic framework [3, 5, 6] which conceptualizes cities as dynamic, interconnected systems where natural and anthropogenic elements coevolve [7]. This paradigm shift demands tools that can synthesize disparate data streams into cohesive 3D representations of urban form and function. To this end, we employ LiDAR-derived digital elevation models (DEMs) and GIS layers to reconstruct high-resolution urban models, capturing features such as building volumetry, vegetation density, and microtopographic variations. These models serve as the training substrate for neural network architectures, including Convolutional Neural Networks (CNNs) for spatial feature extraction and Recurrent Neural Networks (RNNs) for temporal pattern recognition. For example, CNNs trained on LiDAR data can identify unauthorized vertical expansions in informal settlements, while RNNs applied to decadal satellite imagery reveal cyclical land-use transitions in peri-urban zones [8].

A novel contribution of this study lies in its comparative analysis of urban areas undergoing routine development versus those disrupted by extraordinary events, such as military hostilities or climate-induced disasters. In post-war/disaster contexts, neural networks can disentangle patterns of reconstruction from chaotic urban decay, offering insights into systemic resilience [9]. For instance, in cities recovering from earthquakes, our framework distinguishes between planned rebuilding and ad-hoc construction, enabling policymakers to prioritize resource allocation. Similarly, in post-war /post-conflict zones, the detection of subtle morphological changes - such as the emergence of informal barriers or the degradation of green corridors - provides early warnings of socio-ecological fragmentation. Such capabilities are not merely technical advancements but essential tools for fostering equitable urban governance.

**The key objective** of this study is to develop and

validate a neural network-driven framework for analyzing urban morphology changes, leveraging LiDAR and GIS technologies to detect and quantify both routine urban development and disruptions caused by extraordinary events, such as armed conflicts, military hostilities, or natural disasters. As a case study, we focus on the city of Kharkiv, Ukraine, which experienced severe urban disruptions during the first three months of the full-scale Russian invasion (February–April 2022). This period of intense hostilities provides a critical context for examining the resilience and morphological transformations of urban systems under extreme stress.

We have implemented the original concept by integrating two key artificial neural network (ANN) approaches for change detection comparison – so called the “ANN Similarity (Enhanced) method” and the “Latest ANN method” - both of which we developed. They illustrate how different ANN configurations can be used to analyze urban changes from multiple perspectives, providing a more nuanced understanding of the data. Thus, the research seeks to automate the identification of subtle morphological shifts, such as building modifications, vegetation loss, and infrastructure degradation, while providing comparative insights into the resilience and recovery patterns of urban systems. The ultimate goal is to equip urban planners and policymakers with a scalable, AI-enhanced toolset for evidence-based decision-making in sustainable urban development and disaster recovery.

The implications of this work extend beyond the only academic field. Urban planners increasingly face pressure to balance growth with sustainability, particularly in regions grappling with climate vulnerability. By automating the detection of illegal land encroachments or quantifying the carbon sequestration potential of urban forests, our neural network-driven approach equips stakeholders with actionable intelligence for evidence-based decision-making. Furthermore, the scalability of this methodology, applicable to megacities and small towns alike, ensures its relevance across diverse geographic and socio-economic contexts.

Thus, our paper demonstrates how neural networks transcend the limitations of traditional geospatial tools, offering a robust, scalable solution for monitoring urban evolution. By fusing cutting-edge AI with LiDAR and GIS technologies, we advance both the theory and practice of urban morphology analysis, providing a blueprint for smarter, more resilient cities in an era of rapid global change.

**Review of previous works.** The analysis of urban morphology changes has significantly advanced with the integration of neural networks, offering enhanced accuracy and efficiency in detecting and interpreting urban transformations [10–14]. Our shor-

tened literature survey explores the evolution of methodologies in this domain, highlighting key studies and their contributions.

*Early developments in neural network applications.* The application of artificial neural networks (ANNs) in urban change detection began gaining traction in the early 2000s. Pioneering studies, such as those referred to in [10], developed ANN-based methods to identify newly urbanized areas using Landsat Thematic Mapper images from different dates. These approaches often utilized principal component analysis (PCA) to extract salient features, reducing data dimensionality before applying ANNs for change detection [11]. Similarly, research employing ARTMAP neural networks demonstrated effective urban change detection with Landsat TM images, underscoring the potential of neural networks in this field [12]. Subsequent work [13] introduced neural networks to model land-use changes in watersheds, emphasizing their predictive capabilities, while other authors expanded this to multitemporal land cover classification [14].

*Advancements with deep learning techniques.* The evolution of deep learning has further propelled urban morphology analysis. Convolutional Neural Networks (CNNs) have been particularly influential. A notable study introduced a strategy for extracting indicators from large-scale orthoimages of varying resolutions using CNNs, facilitating urban change detection with acceptable accuracy after minimal training [15]. Another innovative methodology combined deep neural networks with inverse modeling to generate urban morphometric parameters, enhancing environmental assessments at the city scale [16]. One of the recent years' works demonstrated CNNs' ability to detect changes in urban sprawl using multi-source remote sensing data, achieving over 90% accuracy [17], and another publication within these years introduced deep learning for morphometric parameter extraction [18]. Recurrent Neural Networks (RNNs), particularly Long Short-Term Memory (LSTM) networks, have also been explored for their temporal modeling capabilities. Research integrating fully convolutional networks with RNNs has shown promise in capturing temporal dependencies in multitemporal Sentinel-2 data [19], with other authors extending this approach by combining LSTMs with attention mechanisms [20].

*Integration of multisource data.* The fusion of optical and Synthetic Aperture Radar (SAR) data has been a focal point in recent studies. A neural network-based framework was developed to detect urban changes using varying numbers of optical and SAR observations, addressing challenges posed by atmospheric effects and seasonal variations [21]. This multisource data integration enhances the robustness of change detection models, which has been increa-

singly explored in recent geospatial research. For instance, some authors proposed a hybrid ANN model combining SAR and LiDAR data to detect subtle urban changes [22], while others demonstrated multi-source fusion for urban monitoring [23].

*Benchmark datasets and methodological innovations.* The creation of benchmark datasets has been pivotal for advancing urban change detection methodologies. The *Hi-UCD dataset*, introduced in the recent years, comprises high-resolution aerial images with semantic annotations across multiple time phases [24]. Methodologically, the adoption of Siamese CNN architectures has facilitated the extraction of features from temporal image pairs [25], and transformer-based neural networks for improved feature extraction have been introduced recently [26]. Earlier surveys systematically reviewed change detection algorithms [27], while some advanced algorithmic solutions were proposed somewhat later, for instance - for continuous land cover classification [28].

*Challenges and Future Directions.* Despite significant progress, challenges persist in the field of urban morphology change detection. Accurately capturing complex urban features and addressing data quality issues remain areas for improvement [29]. Future research may be anticipated to focus on refining neural network architectures, enhancing data fusion techniques, and developing comprehensive benchmark datasets [30]. The development of real-time monitoring systems and integration with geospatial decision-making frameworks will likely be critical in shaping the next generation of urban remote sensing applications.

**Exposition of the main research material. The basics of artificial neural networks for urban studies.** *Constructed (Artificial) Neural Network (ANN)* is essentially a mathematical modeling technique based on the principles of organization and functioning of the human central nervous system, particularly those principles that implement human logic and the ability to solve a wide range of problems, for example, within the urban remote sensing domain [2, 8, 20, 25, 31]. The core content of this modeling technique is the emulation of biological neural networks and the creation of learning algorithms. These algorithms are used in tasks where the application of other logic or analytical techniques is problematic, such as in complex forecasting or pattern recognition tasks.

The ANN methodology differs from other computer modeling techniques primarily in that it *is not rule-based* and does not require a *predefined knowledge base*. An ANN model learns based on associative patterns to recognize and generalize relationships between sets of input and output parameters for modeling and analysis.

In this study we apply to those constructed neural networks, which possess a typical architecture that

includes the following main components: *network topology*, *learning paradigm*, and *learning algorithm*. The *network topology* defines its overall organization, the specifics of node connections, the direction of data flows, and error information between network layers. The *learning paradigm* determines the relationship between the two main learning algorithms that can be used: supervised learning and unsupervised learning.

Our algorithms of comparison employed further in this text have been primarily based on one of the most common ANN algorithms, which is the so-called *multi-layer topology algorithm*, in which all modeling elements (processing units) are organized into three key constituent layers: *input*, *hidden*, and *output* [32]. The *input layer* is designed to transmit predictive attribute data further to the *hidden layer*, which is connected to the *output layer*, where the final results are placed. Within this architecture, the simulated output layer is recursively compared with the desired output results until the delta between them (error signal) is minimized and the results of computer modeling begin to match the desired pattern.

While composing our relevant workflow, we also have taken into account probably the most suc-

cessful definition of the ANN basic principles, which has become a classic over the past two decades, was provided by three authors back in 2000 [33]. This expert believes that artificial neural networks are distributed, adaptive, nonlinear learning machines built from a variety of different elementary neural processors (PEs). Each PE in the network is connected to other processing elements and to itself. This *interconnectivity* defines the *network topology*, which is one of the foundations of its architecture. The information flows passing through the network nodes are scaled by parameters called *weights*,  $w_{ij}$ . The scaled information signals are summed as a collective contribution to the output layer of each PE in the network, and the output layer itself is a nonlinear (static) function. The output signal of each elementary neural processor either becomes part of the overall system output or is summed into the output signal of a neighboring cluster of PEs (i.e., several PEs). Thus, the *classical ANN architecture*, described above on the base of [32, 34], can be stylized, as we understand it, in the following way (Fig. 1).

Thus, seven key points described above due to the ANN-basics for urban studies can be summarized like follows:

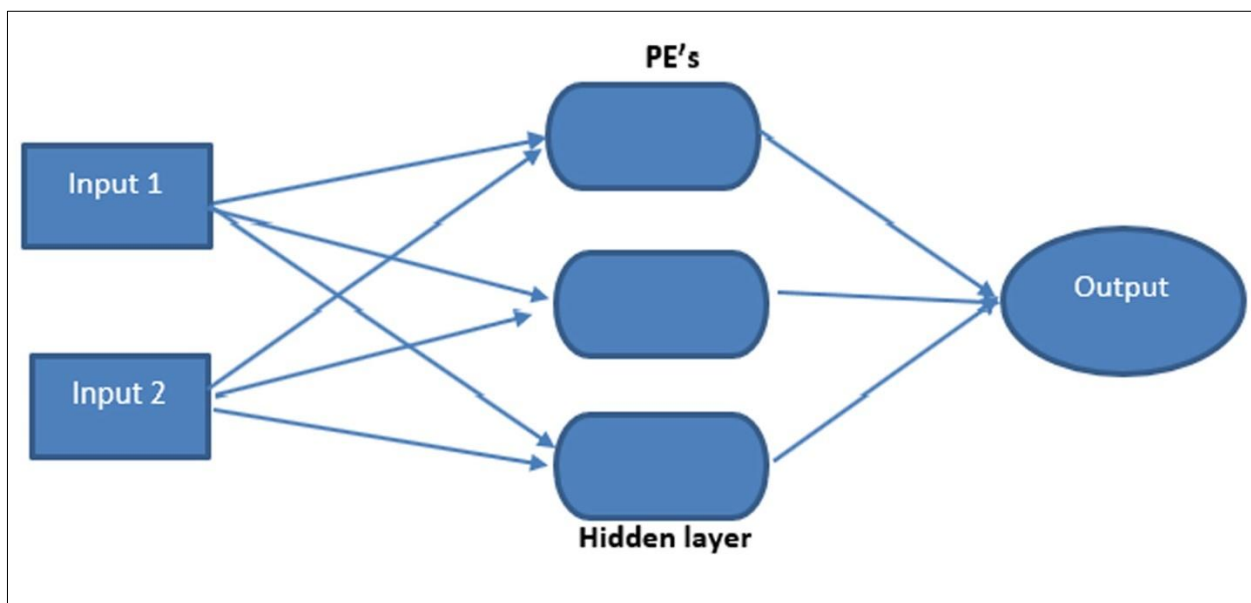


Fig. 1. The classical ANN architecture stylized according to the basics introduced in [32, 34]

1. *ANN as a Modeling Technique*: Based on principles of the human nervous system.
2. *Learning Algorithms*: Used for tasks like forecasting and pattern recognition.
3. *Distinctive Features*: Not rule-based, no pre-defined knowledge base, relies on associative learning.
4. *ANN Architecture*: Comprises topology, learning paradigm, and learning algorithm.
5. *Multi-Layer Topology*: Input, hidden, and output layers with recursive error minimization.
6. *Lefebvre's Definition* [33]: ANNs as distributed, adaptive, nonlinear learning machines.
7. *Interconnectivity and Weights*: Information flows are scaled by weights and summed for output.

**Applications in urban studies.** It is evident according to the basics introduced in the previous subsection, that ANNs can become instrumental in urban studies, offering advanced methodologies to analyze and interpret complex urban systems. ANNs, inspired by the human brain's neural architecture, consist of

interconnected nodes (neurons) that process information using adaptive weights. This structure enables them to model nonlinear relationships and patterns within data, making them particularly suitable for the multifaceted nature of urban environments, what is the premise for these three following applications feasible:

1. *Urban Growth Prediction*: ANNs have been employed to forecast urban expansion by analyzing socio-economic and geographic factors. For instance, a study in Mexico integrated ANNs with cellular automata to predict vertical urban growth, aiding urban planning decisions [34]. This model utilized spatial analysis and image processing to simulate various urban growth scenarios, demonstrating the capability of ANNs to handle complex urban dynamics.

2. *Urban Building Energy Modeling (UBEM)*: In the quest for sustainable cities, ANNs have been applied to model energy consumption patterns in urban buildings. A notable example is the TEAC tool, developed for the Polish residential sector, which leverages ANNs to analyze energy usage [35]. This approach addresses the limitations of traditional UBEM tools by providing tailored analyses for specific urban contexts, thereby enhancing the accuracy of energy consumption predictions.

3. *Smart City Regulation*: The integration of ANNs in smart city frameworks has facilitated real-time monitoring and management of urban systems. One of the referred to research has highlighted the importance of using ANNs to regulate smart cities, ensuring the protection of civic rights, security, and privacy [36]. By processing vast amounts of data from various urban sensors, ANNs can identify patterns and anomalies, contributing to more responsive and adaptive urban management strategies.

Upon any development of a relevant workflow, it is mandatory to realize that despite their advantages, the application of ANNs in urban studies presents challenges. The quality and representativeness of input data are critical, as biases or inaccuracies can lead to flawed outcomes. Moreover, the *black-box* nature of ANNs raises concerns about interpretability, making it essential for urban planners and policymakers to understand the underlying mechanisms of these models. Addressing these challenges requires interdisciplinary collaboration, combining technical expertise with domain-specific knowledge to ensure that ANN applications in urban studies are both effective and trustworthy.

Thus, ANNs offer powerful tools for analyzing and managing urban systems. Their ability to model complex, nonlinear relationships makes them invaluable in various urban applications, from change detection for growth prediction to energy modeling and smart city regulation. As urban areas continue to evolve, the integration of ANNs in urban studies is

poised to play a pivotal role in shaping sustainable and resilient cities.

**Urban remote sensing with LiDAR.** Our research approach to the aforementioned issues aligns with the frameworks of Urban Remote Sensing utilizing LiDAR for digital city modeling [2, 5, 6, 9, 37]. In this paper the central to the approach is our concept of comparing various change detection datasets through ANN analysis.

LiDAR systems are broadly categorized into Airborne LiDAR Systems (ALS), deployed on aircraft, helicopters, or drones (UAVs), and Terrestrial LiDAR Systems (MLS), which are vehicle-based and mobile. While MLS techniques have recently gained prominence, their primary applications extend beyond building facade extraction to include urban road feature recognition [38] and infrastructure network feature extraction using combined ALS/MLS methods [39].

A critical challenge in automated feature extraction lies in establishing seamless integration between mobile LiDAR (MLS) and airborne LiDAR (ALS) datasets. This integration is essential for creating comprehensive 3D urban models. For instance, Figure 2 illustrates the results of a LiDAR project aimed at simulating downtown Ottawa at the end of the first decade of the millennium, based on data provided by the municipality. The author of this paper served as the project's research advisor. This example underscores the potential of combining ALS and MLS datasets for the extraction, recognition, and classification of geographical objects.

LiDAR data is particularly well-suited for simulating and visualizing urban environments through 3D city models. Most existing approaches focus on reconstructing roof and facade levels with varying degrees of accuracy, as depicted in Figure 2B.

These 3D models enable a wide range of highly efficient applications across 14-18 industrial domains, from urban planning to disaster management [4].

**Case study: urban change detection using LiDAR to assess the hostilities' impact.** *Methods and techniques of change detection.* The Change Detection (CD) technique leverages our high polyhedral modeling Building Extraction (BE) from LiDAR point clouds functionality [37] to automate the monitoring of architectural and geometric changes in urban environments over a specified time period. This is achieved by comparing and analyzing *two* LiDAR point clouds, enabling the identification of changes in the positions and shapes of buildings represented as 3D models. Our CD methodology addresses three fundamental tasks essential for accurate 3D change detection:

1. Coordinate system alignment,
2. Spatial and spectral comparison, and
3. Representation and analysis of detected changes.



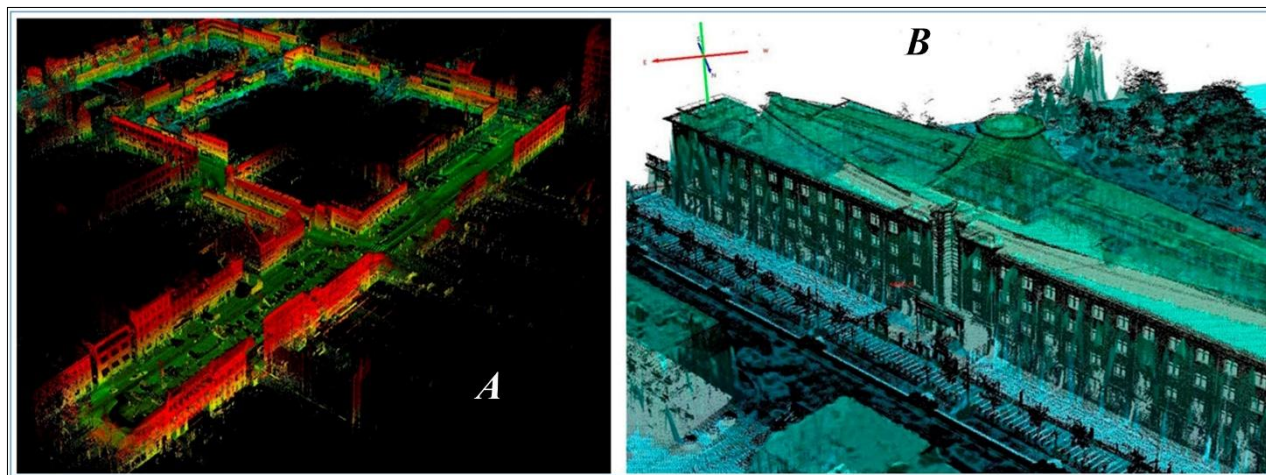


Fig. 2. *A* – ALS/MLS reconstruction of the route of President Obama's visit to Ottawa;  
*B* – MLS-reconstructed facades of the Canadian parliament building.

Furthermore, our approach aligns with established urban change categorization frameworks, which classify changes into three primary categories: positive, negative, and no change, each with subcategories. In our study, the *Added* and *Removed* building change classes correspond to partial change cases, such as "new (part)" and "demolished (part)".

Our proposed CD solution overcomes these challenges by detecting differences between buildings extracted from multitemporal LiDAR Point Clouds aligned to the same geographic extent. Unlike traditional methods, which struggle to distinguish buildings with similar textures from other structures, our approach employs an effective thresholding technique to filter out insignificant changes.

To ensure the accuracy of detected changes, we differentiate between real changes and artifacts (caused by data errors). Artifacts are identified by analyzing point density: if a lot contains points from the *Primary* Point Cloud but none from the *Secondary* point cloud, it is flagged as an artifact. Conversely, real changes exhibit higher point density in the relevant cloud (*Secondary* for *Added* changes, *Primary* for *Removed* changes). This density threshold method effectively discriminates between artifacts and genuine changes.

Finally, the detected changes are classified into three categories:

1. *Unchanged* building lots,
2. *Added* lots (completely or partially covered by new construction), and
3. *Removed* lots (completely or partially demolished buildings).

These classifications are integrated into the *BE*-database, updating the status of buildings within the change detection framework. This approach not only enhances the accuracy of urban change detection but also provides a robust foundation for applications in urban planning, disaster recovery, and policy devel-

opment.

Desktop software. The proprietary *iQ City Change Management (CCM)* software, a desktop application for *Windows OS*, was developed under the leadership and primary contribution of the author as a non-commercial project without external funding. The software's algorithmic core was implemented using *C++* and *Python*, while the user interface was developed with *C# MS .NET*. Initially introduced in an academic publication detailing urban studies with LiDAR data processing in the Kharkiv region [5], the software underwent its latest update in 2019, with the algorithmic core adapted for *C++ 11* and *Python 3.7*.

The *CCM* software features an intuitive user interface. Upon launching, users can either access recently completed projects via *File => Recent Projects* or initiate a new project. For new projects, users configure parameters in the *Project Preferences* dialog, including selecting a projection system from the supported categories and adjusting additional settings under the *General* option. Once project setup is complete, raw *.LAS* files are imported for processing. Within the framework of high polyhedral modeling, users sequentially apply *BE* and *CD* functionalities. The *Workbench* menu provides access to the *Building Extraction Technology* tool (Fig. 3), which offers three options for detecting and extracting buildings. These options also identify changes in urban features, exporting results as *.OBJ* and *.ThreeDFM* files.

Initial LiDAR datasets and visualization of detected changes. The *Primary Kharkiv Northern Saltivka (KHNS)* dataset was collected by the surveying Company in June 2019 using a *Riegl VQ-1560 II-S* sensor mounted on a helicopter, covering a 68 sq. km urban area. A 4 sq. km test site within this area, containing approximately 122 million points, served as the focus for analysis. The raw ALS data was preprocessed using *Riegl RiProcess* software, with the resulting colored point clouds exported as *.LAS 1.4* files.

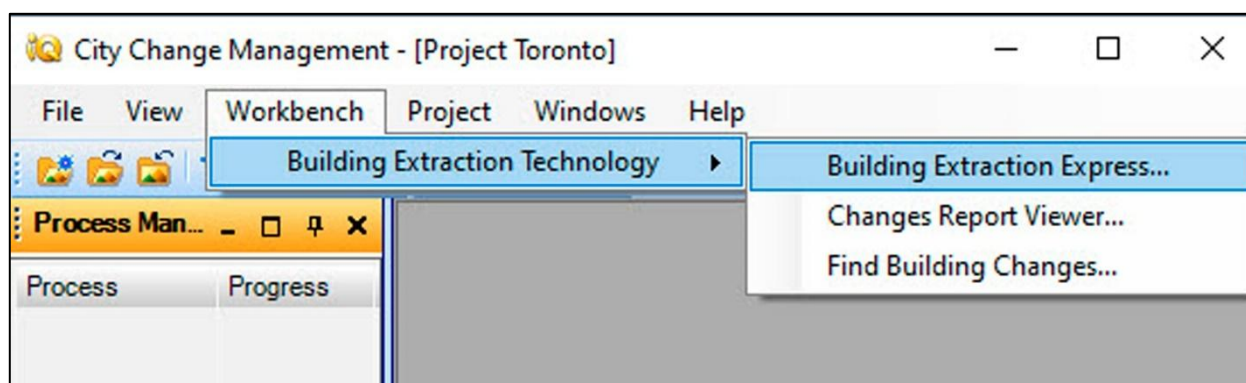


Fig. 3. *Workbench* menu in the *CCM* interface that starts BE and CD procedures consequently

Unlike previous work in North America, where preprocessed ALS/MLS datasets were provided by local authorities, this study faced the challenge of processing raw LiDAR data. While a helicopter was used for ALS data collection, attempts to gather MLS data for building facades using a land vehicle were unsuccessful. Despite advanced methods for combining ALS/MLS point clouds [40], a sustainable composite dataset for model calibration within the high polyhedral modeling workflow could not be achieved.

Following the cessation of violent conflicts in Kharkiv's outskirts in September 2022, the need for URS to support post-war recovery became a priority for local government, researchers, and NGOs. With permission from local authorities, our volunteer team conducted a second ALS survey in mid-November 2022 on exactly the mentioned above 4 sq. km but now deserted urban zone, using the same equipment and preprocessing software donated by the Company.

For comparative analysis we have sought for urban sites not struck by the hostilities, but faced a routine redevelopment. LiDAR data from two locations in Tallinn, Estonia, were obtained from the national geoportal [41]. Each of these locations was 4 sq. km too. The *Primary* surveys in December 2017 produced datasets *Estonia-1/Estonia-2* (*EST-1/EST-2*), approximately 80 million points each, with an average density of 20 points/sq. m. The *Secondary* surveys in December 2022 yielded 120 million points per dataset, with a density of 30 points/sq. m. While the *KHNS* dataset spans a 3-year change detection gap, the Tallinn datasets cover 5 years, posing potential accuracy challenges.

Thus, using ALS data from 2017 and 2022 for the *EST1* and *EST2* datasets, and from 2019 and 2022 for the *KHNS* dataset, we generated differences in BE models between primary and secondary segments using the described BE and CD techniques [9].

The areal distribution of detected changes for *EST1*, *EST2*, and *KHNS* was calibrated using additional repeated ALS datasets, as mentioned in Fig. 3 (Toronto project in a window caption of the *CCM*

interface). For the primary focus of this research, urban morphology changes in the *KHNS* site of Kharkiv were analyzed, including a visual comparison of CD areal distributions across the three key study sites (4 sq. km each) (Fig. 4-6). Detected changes were visualized alongside intact building models as *3D scenes*, providing a more representative depiction than simplified 2D schemes, particularly when outlining multiple types of building changes.

The footprints of extracted buildings, the centroids of CD features, and a topographic grid generated by *CCM* were exported to *QGIS* as raster layers and point/polygonal feature sets. While *CCM* could not visualize CD footprints for export, precise numerical values (**Area** - *A*, **Volume** - *V*, **Height** - *H*) of these features were computed and used to map CD centroids in this full format GIS - *QGIS*. Using *X*, *Y* coordinates from a *CCM*-generated *.CSV* file, the *Select by Location* tool in *QGIS* identified building footprints intersecting CD centroids. This approach enables users to detect changed buildings and create a separate CD layer with the key attributes mentioned (*A*, *V*, *H*) even without specialized software like *CCM*.

***ANN analysis for comparing detected urban changes' datasets. Some introductory issues.*** Choosing three basic geometric change parameters (*Area*, *Volume*, and *Height*) for ANN analysis in *Wolfram Mathematica 13.2* is a logical approach to formalize data regularities and classify detected changes. The number of these changes, which determine derivative datasets, is like follows:

- ***EST-1***: 48 *Added* CD features and 67 *Removed* ones;
- ***EST-2***: 175 *Added* CD features and 174 *Removed*;
- ***KHNS***: 215 *Added* CD features and 51 *Removed*; all *Removed* CD objects in *KHNS* could be supposedly caused by the military impact only.

However, selecting an appropriate quantitative method posed challenges, as these data do not clearly belong to either natural or social science domains. To



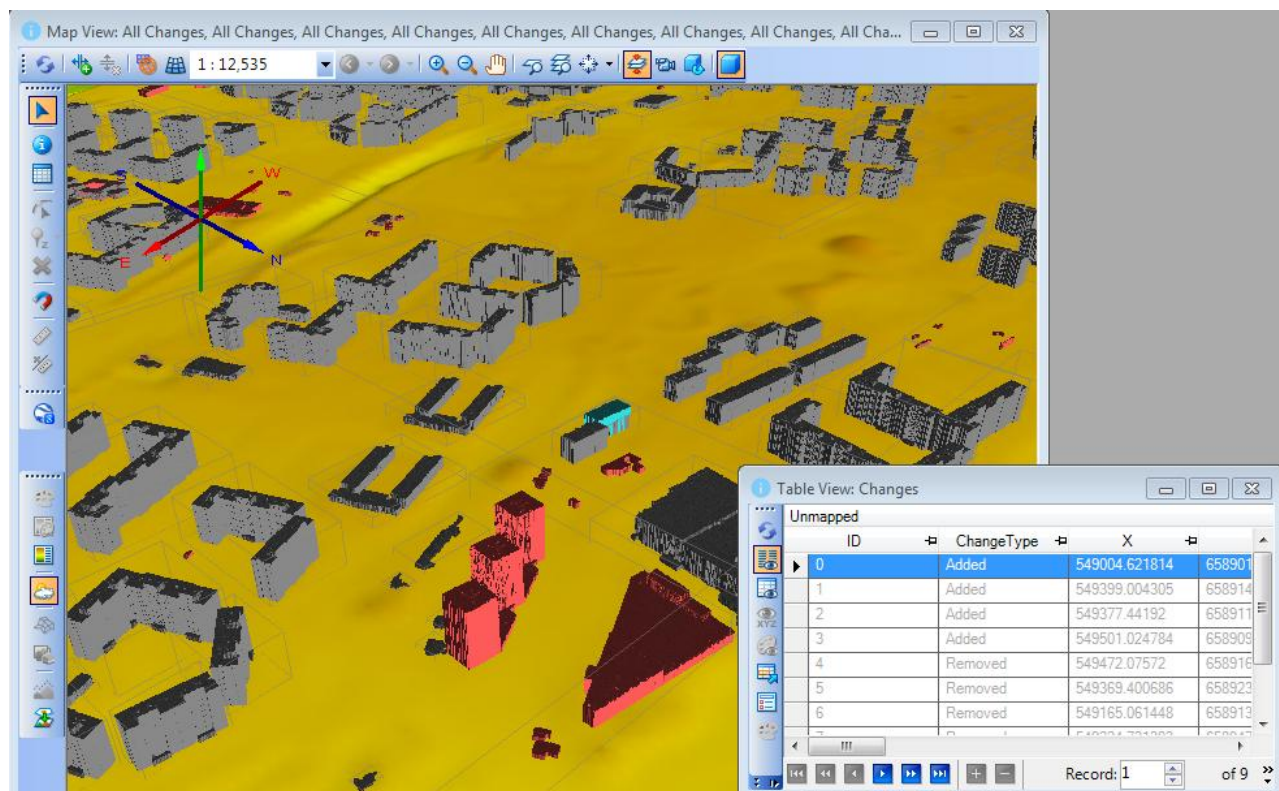


Fig. 4. Results of change detection in the CCM interface for the multitemporal (2017–2022) LiDAR dataset *EST1*: Lasnamäe city district, Tallinn. Detected changes in architectural morphology are highlighted in red

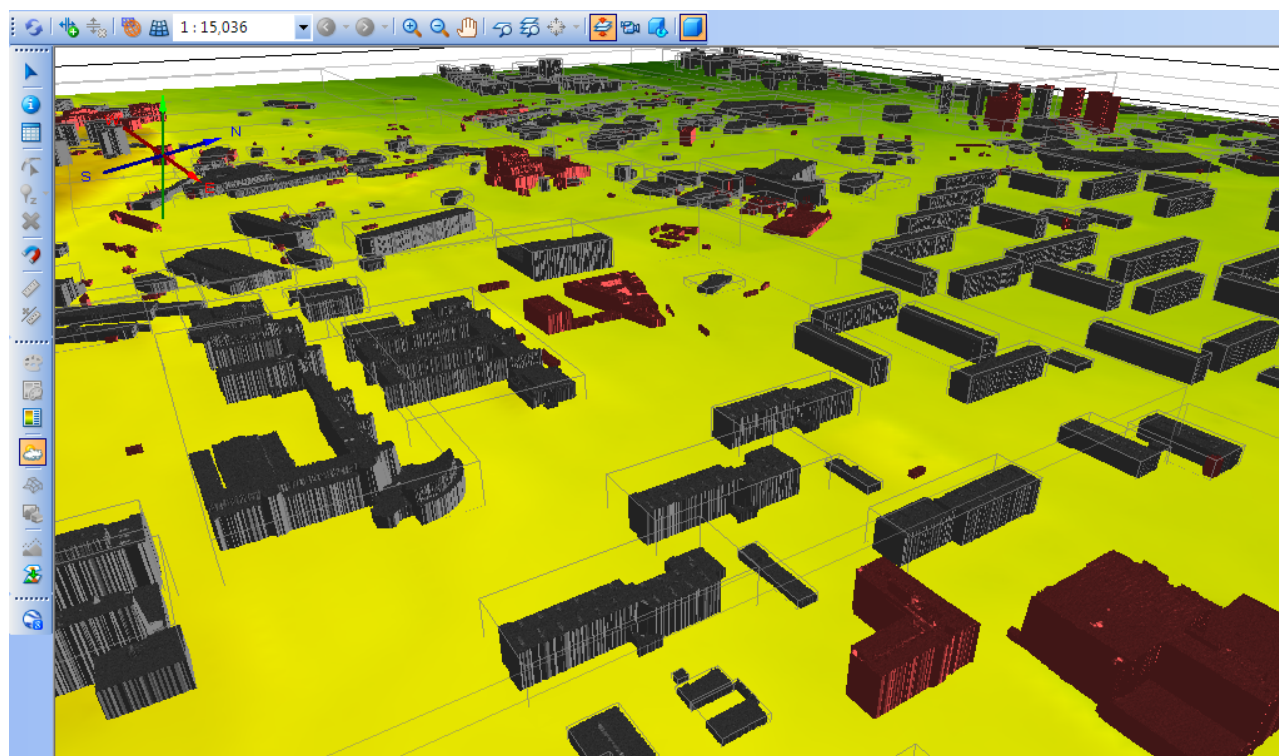


Fig. 5. Results of change detection in the CCM interface for the multitemporal (2017–2022) LiDAR dataset *EST2*: Mustamäe city district, Tallinn. Detected changes in architectural morphology are highlighted in red



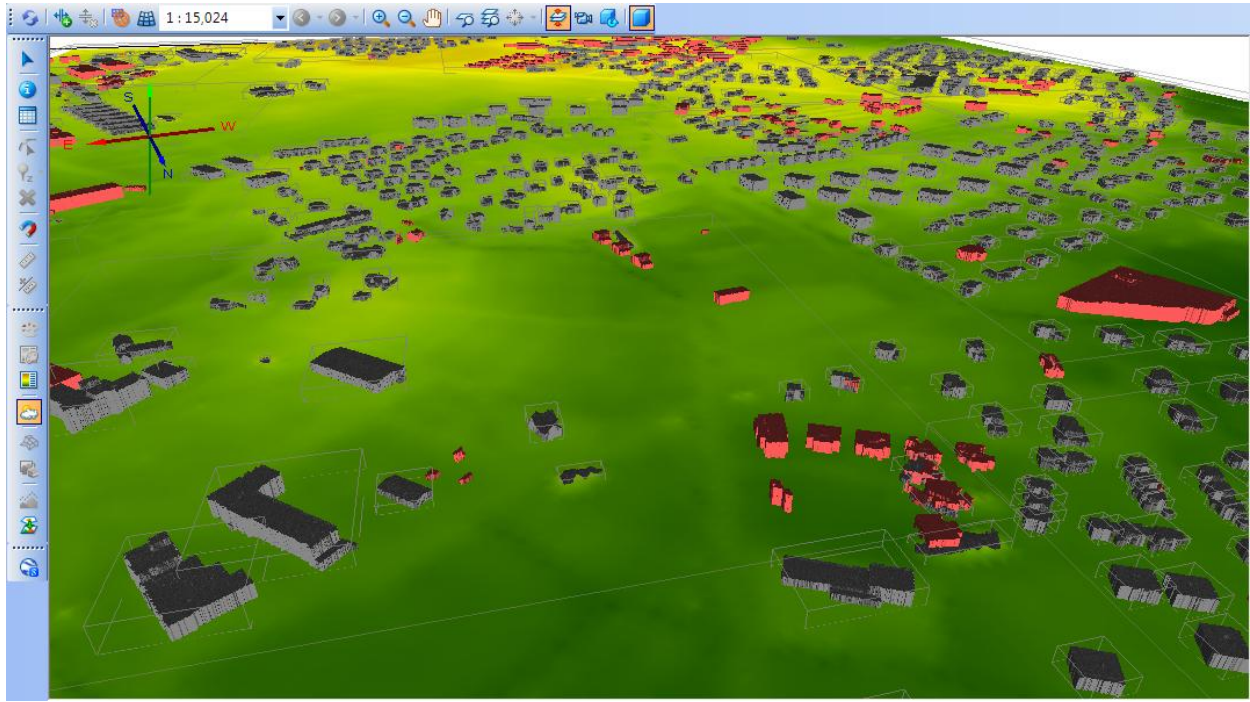


Fig. 6. Results of change detection in the CCM interface for the multitemporal (2019–2022) LiDAR dataset KHNS: Northern Saltivka city district, Kharkiv.  
Detected changes in architectural morphology are highlighted in red

address this, we considered existing examples of statistical evaluation within the building change detection domain, such as approaches validating demolition statistics (e.g., the number and volume of demolished buildings) [42].

Our research ANN outline. Our ultimate task is to compare, through neural network analysis using Wolfram Language, the following datasets:

- Positive changes (class *Added*): *EST1n*, *EST2n*, *KHNSn*.
- Negative changes (class *Removed*): *EST1Rn*, *EST2Rn*, *KHNSRn*.

Each dataset consists of arrays of geometric objects with three columns representing *Area*, *Volume*, and *Height* (*A*, *V*, *H*) without explicit labels. We assigned:

- Labels 1, 2, and 3 to positive changes (*EST1n*, *EST2n*, *KHNSn*), corresponding to newly built buildings or their parts.
- Labels 4 and 5 to negative changes (*EST1Rn*, *EST2Rn*), corresponding to demolished buildings from normal urban redevelopment.
- Label 6 to negative changes (*KHNSRn*), corresponding to demolished buildings due to military hostilities.

We aim to compare the following pairs to identify differences or similarities:

1. Positive pairs: *EST1n* with *EST2n*, *EST1n* with *KHNSn*, *EST2n* with *KHNSn*.
2. Negative pairs: *EST1Rn* with *EST2Rn*, *EST1Rn* with *KHNSRn*, *EST2Rn* with *KHNSRn*.

For this purpose, we created paired datasets:

- Positive pairs: *pairsEST1nEST2n*, *pairsEST1nKHNSn*, *pairsEST2nKHNSn*.
- Negative pairs: *pairsEST1RnEST2Rn*, *pairsEST1RnKHNSRn*, *pairsEST2RnKHNSRn*.

Each pair provides a unique numerical value for "similar-dissimilar" comparison through binary classification. These six datasets serve as inputs, each containing pairs of values for comparison.

After loading and labeling the datasets, we generated six *adjusted* datasets:

- *adjustedTestSetEST1nEST2n*, *adjustedTestSetEST1nKHNSn*, *adjustedTestSetEST2nKHNSn*.
- *adjustedTestSetEST1RnEST2Rn*, *adjustedTestSetEST1RnKHNSRn*, *adjustedTestSetEST2RnKHNSRn*.

Using these adjusted datasets, we created *trainingData* and *validationData* variables, manually editing each dataset to ensure a consistent format of six features followed by one label. All datasets were saved as .CSV files in a specified directory.

Crucially, we incorporated insights from prior research based on statistical data and model analysis, which provided expected similarity/dissimilarity outcomes for the pairs [9], each of them forms the corresponding classes of the future comparison:

- *EST1n* with *EST2n*: Expected to be similar, classes 1, 2 of the future comparison.
- *EST1n* with *KHNSn*: Expected to be similar, classes 1-3.

- *EST2n* with *KHNSn*: Expected to be slightly dissimilar, classes 2-3.
- *EST1Rn* with *EST2Rn*: Expected to be similar, classes 4-5.
- *EST1Rn* with *KHNSRn*: Expected to be dissimilar, classes 4-6
- *EST2Rn* with *KHNSRn*: Expected to be marginally dissimilar, classes 5-6.

Workflow for comparing datasets using neural networks. To achieve the goal of comparing six pairs of datasets and obtaining a unique numerical value indicating their similarity or dissimilarity, the following workflow was implemented:

*Step 1: Data Preparation:*

1. Load Datasets: Ensure all six datasets are properly loaded and formatted. Each dataset should consist of six features (representing geometric parameters: *Area*, *Volume*, and *Height*) followed by one label (indicating the class of change).
2. Data Formatting: Verify that the datasets are structured consistently, with each row containing six feature values and a corresponding label. Save the datasets as *.CSV* files for compatibility with the neural network framework.

*Step 2: Neural Network Training:*

1. Model Design: Train a neural network for each pair of datasets to perform binary classification, distinguishing between similar and dissimilar pairs.
2. Training Process: Use the prepared datasets to train the neural network, ensuring that the model learns to accurately classify the pairs based on their geometric features.

*Step 3: Model Evaluation and Similarity Scoring:*

1. Model Evaluation: Evaluate the trained neural network models using validation datasets to determine their classification accuracy.
2. Similarity Scores: Use the accuracy scores as indicators of similarity or dissimilarity. Higher accuracy suggests greater similarity (indicating the model can easily classify the pair as similar), while lower accuracy suggests greater dissimilarity (indicating the model struggles to classify the pair as similar).
3. Aggregate Measure: Calculate a *totalAccuracy* metric to provide a combined measure of similarity/dissimilarity across all pairs.

*Interpretation of Results*

- Unique Numerical Values: The accuracy scores for each pair serve as unique numerical values quantifying their similarity or dissimilarity.
- Comparative Analysis: *Higher accuracy* values indicate *greater similarity* between datasets, while *lower* values indicate *greater*

*dissimilarity*. This approach enables a systematic comparison of urban change datasets, providing insights into their underlying patterns and relationships.

By following this workflow, unique numerical values (accuracy scores) are obtained for each pair of datasets, facilitating a robust analysis of their similarities and differences based on neural network classification.

Proposed methodology for multi-class neural network analysis, neural network architecture, and its implemented classification. Taking into account all stated above so that to address the task of comparing urban morphology datasets, the following finally approach is proposed:

1. *Label Definition*: the datasets are labeled as *1*, *2*, and *3* for positive changes (e.g., newly constructed buildings) and *4*, *5*, and *6* for negative changes (e.g., demolished buildings). The neural network must output probabilities or scores corresponding to these labels, enabling precise classification of urban changes.
2. *Network Architecture Adjustment*: the neural network architecture is modified to accommodate multi-class classification. Specifically, the output layer is expanded to include *6 neurons*, each representing one of the defined labels. A *Softmax activation function* is applied to ensure that the output probabilities sum to 1, facilitating interpretable class predictions.
3. *Training Process*: the network is trained using the labeled datasets. A *categorical cross-entropy loss function* is employed to optimize the model for multi-class classification, alongside an appropriate optimizer (e.g., Adam) to ensure efficient convergence.
4. *Model Evaluation*: the trained network is evaluated using the adjusted test sets (e.g., *adjustedTestSetEST1nEST2n*). Performance metrics such as *accuracy*, *precision*, *recall*, and *F1-score* are calculated to assess the model's ability to correctly classify urban changes.
5. *Dataset Comparison*: the trained network is applied to predict similarities and differences between paired datasets (e.g., *EST1n* with *EST2n*). The predictions are analyzed to identify patterns of similarity or dissimilarity, providing insights into the nature of urban changes across different contexts.

This finalized methodology ensures a robust and interpretable framework for analyzing urban morphology changes, leveraging the strengths of neural networks to automate and enhance the classification process.

The neural network developed in *Wolfram Mathematica* interface employs a *sequential architecture* designed to process multi-dimensional urban mor-

phology data, such as LiDAR-derived geometric features (e.g., building footprints, heights, or volumetric changes) [Fig. 7]. The architecture is structured as follows:

1. *Input Layer*: accepts 3D data arrays (size:  $67 \times 2 \times 3$ ), representing spatial and temporal features of urban changes.
2. *Flatten Layer*: converts the input into a 1D vector (size: 420) for compatibility with subsequent layers.
3. *Hidden Layers*: A series of linear layers interspersed with *ReLU* (Ramp) activation func-

tions progressively reduce dimensionality ( $100 \rightarrow 50 \rightarrow 10$  nodes), enabling hierarchical feature extraction.

4. *Output Layer*: A final linear layer maps the extracted features to a scalar output (size: 1), which quantifies detected changes (e.g., similarity scores or regression targets).

This architecture is optimized for *binary classification* or regression tasks, such as distinguishing between routine urban redevelopment and war-(conflict-) induced disruptions. The use of *ReLU* activations ensures non-linear modeling capabilities, criti-

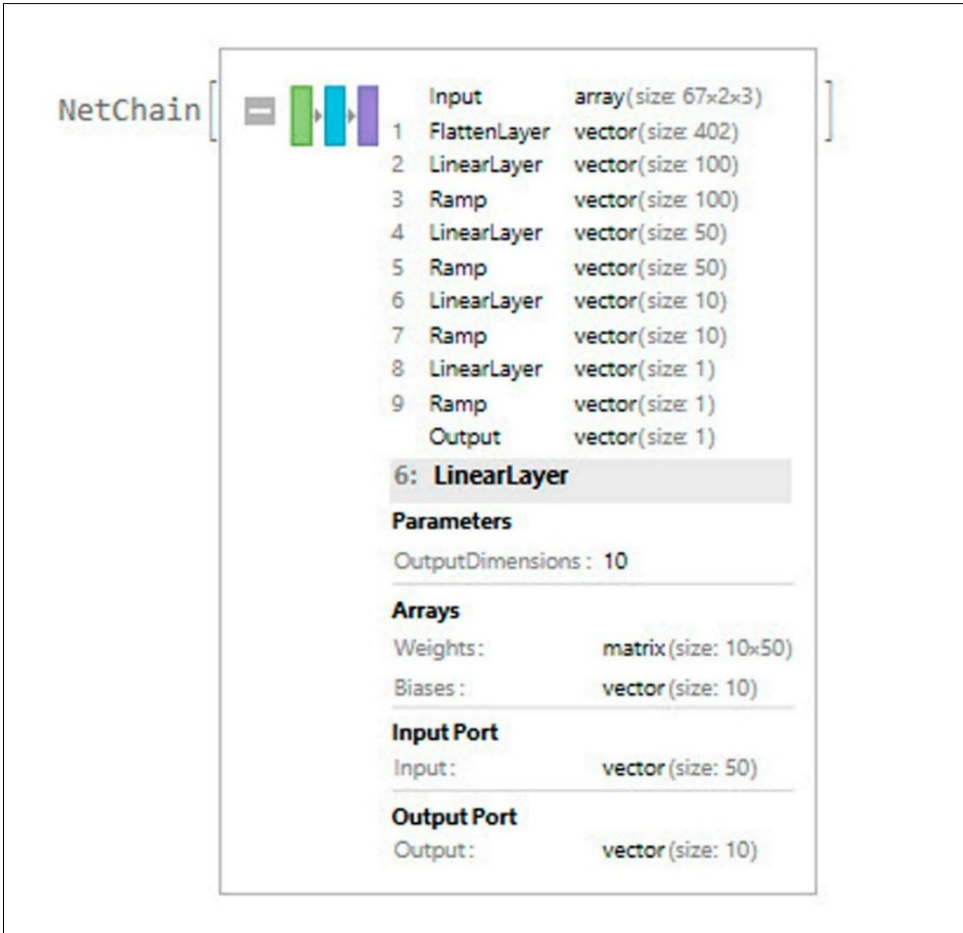


Fig. 7. Neural network architecture for urban morphology analysis: the *Wolfram Mathematica 13.2* interface

cal for capturing complex urban patterns. Its relevance to urban morphology lies in the following:

- *Input Flexibility*: the 3D input structure aligns with LiDAR point cloud data, facilitating analysis of volumetric changes (e.g., demolished or reconstructed buildings).
- *Scalability*: the network’s progressive dimensionality reduction enables efficient processing of large-scale urban datasets.
- *Interpretability*: outputs (e.g., *similarity scores*) provide actionable insights for urban planners, such as identifying zones requiring post-war (conflict) recovery.

This framework underscores the potential of ne-

ural networks to automate and enhance urban change detection, bridging gaps in traditional GIS-based methods.

The following illustrated table represents an implementation of a neural network-based classification system for analyzing urban morphology changes (Fig. 8). The structure showcases a comparison of image pairs processed using a *Siamese Neural Network* framework, where features are extracted via a *NetChain* model.

The output predictions are numerical values that are subsequently thresholded ( $\geq 0.5$ ) to classify pairs as either “*Similar*” or “*Dissimilar*”.

Two latest illustrations are closely linked in that

Figure 7 shows the *neural network architecture* (the *NetChain*), while Figure 8 displays the *classification results* generated by that very architecture. Specifically, the table in Figure 7 illustrates how each pair of inputs mentioned above is processed by the *NetChain*, producing a numeric “Prediction” that is thresholded to classify pairs as either “Similar” or “Dissimilar.” Meanwhile, Figure 7 provides a sche-

matic breakdown of the layers within the *NetChain - FlattenLayer, LinearLayer, Ramp*, and so on—indicating how the input data flows through the network to arrive at those classification outputs. Thus, the two figures together depict both the *structure* of the neural model (Fig. 7) and the *outcomes* it yields when applied to pairs of urban morphology data (Fig. 8).

(←Display the results in a table←)

TableForm[results, TableHeadings → {None, {"Pairs", "Prediction", "Classification"}}]













"Pairs"	"Prediction"	"Classification"
"pairsEST1nEST2n"	NetChain [  ]	If [ NetChain [  ] ≥ 0.5, "Similar", "Dissimilar" ]
"pairsEST1nKHNSn"	NetChain [  ]	If [ NetChain [  ] ≥ 0.5, "Similar", "Dissimilar" ]
"pairsEST2nKHNSn"	NetChain [  ]	If [ NetChain [  ] ≥ 0.5, "Similar", "Dissimilar" ]
"pairsEST1RnEST2Rn"	NetChain [  ]	If [ NetChain [  ] ≥ 0.5, "Similar", "Dissimilar" ]
"pairsEST1RnKHNSRn"	NetChain [  ]	If [ NetChain [  ] ≥ 0.5, "Similar", "Dissimilar" ]
"pairsEST2RnKHNSRn"	NetChain [  ]	If [ NetChain [  ] ≥ 0.5, "Dissimilar", "Similar" ]

Fig. 8. Neural network-based classification scheme for analyzing urban morphology: the *Wolfram Mathematica 13.2* interface

In the context of urban morphology CD, this approach allows automated identification of structural modifications over time. The table suggests that the system is trained to compare spatial and spectral differences in urban point cloud, which is crucial for detecting new developments, demolitions, or transformations in the built environment. We can suppose that this developed methodology may be particularly valuable when working with the variety of sources: high-resolution satellite imagery, LiDAR datasets, or UAV-based urban monitoring systems [43, 44]. The table format indicates a structured workflow where each pair undergoes feature extraction and similarity assessment, demonstrating the robustness of artificial neural networks in spatial-temporal analysis. For future improvements, integrating transformer-based architectures or hybrid deep learning models could enhance feature extraction capabilities, improving accuracy in detecting subtle urban changes.

Two different ANN analysis methods built on the presented network architecture and classification scheme. The previously discussed ANN architecture (and its relevant classification scheme) is our developed variation of a standard feedforward neural network (FNN) with input, hidden, and output layers using *ReLU* and sigmoid activations [45]. It served as the foundation for two new ANN analysis methods elaborated one by one. The so-called *ANN Similarity (Enhanced)* (ANSE) method builds directly on this

architecture, retaining the FNN structure but refining its application to similarity tasks. It employs a Mean Squared Error (MSE) loss for training and computes similarity scores using cosine similarity, ideal for matching dataset pairs. In contrast, the *Latest ANN* (LANN) method extends the architecture significantly by incorporating deeper layers, advanced components like convolutional/recurrent layers (for spatial or sequential data), and activation variants such as *Leaky ReLU*. This method shifts focus to dissimilarity measurement, leveraging contrastive loss with a margin hyperparameter and Euclidean distance for embeddings. While the ANSE-method prioritizes straightforward similarity scoring, the LANN-method emphasizes complex data handling and dissimilarity optimization, making it suitable for tasks requiring nuanced differentiation. Both methods inherit core principles from the original FNN but diverge in complexity, loss functions, and application goals - ANSE for simplicity and similarity, LANN for depth and dissimilarity-driven scenarios.

Previously key premises of these two methods have been illustrated (Fig. 7 and Fig. 8). Figure 7 displays a schematic of the *NetChain* architecture itself. Here, the network is shown to include multiple layers - *FlattenLayer, LinearLayer, Ramp* (activation) layers, and an *Output* layer. This design corresponds to the backbone of the ANSE approach, where a MSE or other standard loss function (such as cross-



entropy) could be used to train the model on labeled pairs. In this configuration, the network's primary objective is to minimize the difference between predicted and actual similarity scores, thereby honing its ability to distinguish between similar and dissimilar inputs.

Meanwhile, Figure 8 shows, as it was already mentioned above, a table of classification results generated by a trained *NetChain* model. This table indicates whether pairs of datasets (e.g., image pairs) are predicted as "Similar" or "Dissimilar." The predictions are numerical outputs that are then thresholded at a predefined value (0.5 in this example). When the output exceeds this threshold, the pair is classified as "Similar," and otherwise as "Dissimilar." This table effectively demonstrates how the ANSE-method processes inputs to yield discrete similarity judgments.

Building on these foundations, the LANN-method modifies certain aspects of the architecture and loss function to emphasize dissimilarity more explicitly. For instance, the margin-based contrastive loss described in the accompanying text highlights how the network can measure the distance between embeddings of two datasets, such as images or LiDAR point clouds. This distance-driven approach can be particularly advantageous when the goal is to detect subtle changes or anomalies, as it focuses on capturing dissimilar features. The Latest ANN method may also incorporate additional layers, such as convolutional or recurrent layers, to handle more complex data structures.

There is formalized content of these two methods to be compared in two following subsections.

#### Formalized content of the ANSE-method.

##### Its ANN architecture:

This method typically uses a feedforward neural network (FNN) with multiple layers. The architecture includes:

- *Input Layer:*  $X=[x_1, x_2, ..., x_n]$ , where  $x_i$  represents features from the dataset;
- *Hidden Layers:* These layers transform the input data using activation functions.
- *Output Layer:* Produces the final prediction or similarity score.

##### Forward propagation:

The neural network processes the input through each layer. For a single layer  $l$ :

1. *Linear transformation:*

$$Z^{(l)} = W^{(l)} \times A^{(l-1)} + b^{(l)}, \quad (1)$$

where:  $W^{(l)}$  is the weight matrix for layer  $l$ ;  $A^{(l-1)}$  is the activation from the previous layer;  $b^{(l)}$  is the bias term.

2. *Activation function:* a common choice is the *ReLU (Rectified Linear Unit)*:

$$A^{(l)} = \text{ReLU}(Z^{(l)}) = \max(0, Z^{(l)}), \quad (2)$$

For the output layer, the activation could be a sigmoid function if the task is binary classification:

$$\bar{y} = \delta(Z^{(l)}) = \frac{1}{1+e^{-Z^{(l)}}}. \quad (3)$$

##### Loss Function:

The loss function measures the difference between the predicted output  $\bar{y}$  and the actual output  $y$ . For similarity, a common choice is MSE:

$$L = \frac{1}{m} \sum_{i=1}^m (\bar{y}_i - y_i)^2, \quad (4)$$

where  $m$  is the number of examples in the dataset.

##### Optimization:

The network minimizes the loss function using an optimization algorithm such as *Stochastic Gradient Descent (SGD)*:

$$W^{(l)} := W^{(l)} - \alpha \times \frac{\partial L}{\partial W^{(l)}}, \quad (5)$$

where  $\alpha$  is the learning rate;  $\frac{\partial L}{\partial W^{(l)}}$  is the gradient of the loss with respects to the weights.

##### Similarity measurement:

After training, the network outputs similarity scores for dataset pairs. These scores may be compared using *cosine similarity*:

$$\text{Cosine Similarity}(A, B) = \frac{A \times B}{\|A\| \|B\|}, \quad (6)$$

where  $A$  and  $B$  are the output vectors for two datasets.

Thus, expressions (1)-(6) represent the formalized framework of the ANSE-method, which combines regression-based learning with neural feature transformation, enhancing the model's ability to capture nuanced relationships in the data. However, the obtained results of the classification comparison did not align with the derivatives of the statistical analysis from [9]. Consequently, we developed some alternative method to address this discrepancy.

##### Formalized content of the LANN-method. Its ANN architecture:

The second developed method could involve a more complex neural network architecture, possibly incorporating deeper layers, different types of layers (e.g., convolutional or recurrent layers), or additional regularization techniques.

##### Forward Propagation:

Similar to the ANSE method, but the architecture might include more sophisticated components:

1. *Deeper Network:* more layers with the same forward propagation equations:

$$Z^{(l)} = W^{(l)} \times A^{(l-1)} + b^{(l)}, \quad (7)$$

$$A^{(l)} = \text{ReLU}(Z^{(l)}), \quad (8)$$

where  $Z^{(l)}$  - output feature map of layer  $l$  after linear transformation;  $W^{(l)}$  - Kernel/filter matrix (learnable weights) that detects spatial patterns (e.g., edges, textures);  $A^{(l-1)}$  - the input activation map from the

previous layer (or raw input data for the first layer);  $b^{(l)}$ : *Bias term* added to each element of the output feature map.

Alternative activations like *Leaky ReLU*:

$$\text{Leaky ReLU}(Z^{(l)}) = \max(0.01Z^{(l)}, Z^{(l)}), \quad (9)$$

## 2. Advanced Layers:

- *Convolutional Layers* (if used for spatial data):

$$Z^{(l)} = W^{(l)} * A^{(l-1)} + b^{(l)}, \quad (10)$$

where  $*$  denotes the convolution operation, where the kernel slides over  $A^{(l-1)}$  to compute dot products at each spatial location.

- *Recurrent Layers* (if used):

$$h_t = \tanh(W_h \times h_{t-1} + W_x \times x_t + b), \quad (11)$$

where  $h_t$  – hidden state at time step  $t$ ;  $h_{t-1}$  – hidden state from the previous time step;  $x_t$  – input at time step  $t$ ;  $W_x$  – weight matrix for the input;  $b$  – bias term; *tanh*: hyperbolic tangent activation function (common in RNNs).

## Loss Function:

In this method, the loss function could be designed to emphasize *dissimilarity*. One possible choice is *Contrastive Loss*:

$$L = \frac{1}{m} \sum_{i=1}^m y_i \times D^2 + (1 - y_i) \times \max(0, \text{margin} - D)^2, \quad (12)$$

where  $D$  is the Euclidean distance between the output embeddings of the dataset pairs; *margin* is a hyperparameter defining the margin for dissimilarity.

## Optimization:

The network parameters are optimized using similar techniques, such as *SGD* as in (5) or *Adam* optimizer:

$$W^{(l)} := W^{(l)} - \alpha \times \frac{\partial L}{\partial W^{(l)}}. \quad (13)$$

The gradients are calculated based on the chosen loss function.

## Dissimilarity Measurement:

The final score reflects *dissimilarity*, which could be derived from the contrastive loss or another metric like *Euclidean distance* between the output vectors:

$$D(A, B) = \|A - B\|, \quad (14)$$

where  $A$  and  $B$  are the output vectors for two datasets.

The formalized content of the LANN-method represents by expressions (7)-(14) *dissimilarity-driven learning*, leveraging specialized architectures and loss functions to distinguish complex or structured data (e.g., images, sequences), contrasting with the earlier similarity-focused regression approach implemented in the ANSE-method.

## Results of datasets' analytical comparison.

Thus, it would be reasonable to emphasize once again, that the essence of our *ANN Similarity (Enhanced)* method lies in using a feedforward neural network to predict similarity scores between dataset pairs, while the essence of the *Latest ANN Method* lies in its focus on *learning dissimilarity* between dataset pairs using a more complex architecture and specialized loss functions.

We integrated the latest score values from our Wolfram code output into the following analysis. These scores represent another from [9] dimension of comparison, reflecting the similarity or dissimilarity between the dataset pairs based on the two methods introduced above in details. We used the same nominal classes of pairs designated in the *Our research outline* subsection and obtained the following results in the *Wolfram Mathematica* interface due to the LANN-method. These pairs' classes have been titled with the following thematic content (Fig. 9):

The comparative analysis of the scores obtained from both methods is like follows:

Final Results:			
Classes	Relationship	Score	Interpretation
Out[62]=	1-2 New Developments Similarity	0.66	Moderate Similarity
	1-3 New-Heritage Comparison	0.60	Moderate Similarity
	2-3 New Development Dissimilarity	0.35	Different Characteristics
	4-5 Demolition Pattern Similarity	0.74	Moderate Similarity
	4-6 Conflict Zone Contrast	0.32	Different Characteristics
	5-6 Demolition Type Differentiation	0.42	Different Characteristics

Fig. 9. Similarity-Dissimilarity scores of urban morphology changes according to the LANN-method: the *Wolfram Mathematica 13.2* interface

1. *EST1n vs. EST2n – New Developments Similarity* pair class:
  - *ANN Similarity (Enhanced)*: 0.894851 (High Similarity);

- *Latest ANN method score*: 0.664566 (Moderate Similarity through Dissimilarity measures);

Analysis: The low dissimilarity score from the

LANN-method indicates that the datasets are very similar in the context of the that approach. This aligns with the high similarity detected by the first method.

**2. *EST1n* vs. *KHNSn* – New-Heritage Comparison pair class:**

- *ANN Similarity (Enhanced)*: 0.522459 (Moderate Similarity);
- *Latest ANN method score*: **0.606253** (Moderate Similarity through Dissimilarity measures);

**Analysis:** Similar to *EST1n* vs. *EST2n*, the LANN method reveals a low dissimilarity score, suggesting significant underlying similarity. This low dissimilarity might indicate that the datasets share certain trends or patterns, possibly related to specific features that the ANN captures.

**3. *EST2n* vs. *KHNSn* – New Development Dissimilarity pair class:**

- *ANN Similarity (Enhanced)*: 0.821002 (High Similarity);
- *Latest ANN method score*: **0.351065** (Different Characteristics – Moderate Dissimilarity through Dissimilarity measures)

**Analysis:** The moderate dissimilarity score from the latest method suggests that *EST2n* and *KHNSn* are relatively dissimilar, what correspond to our preliminary research [9]. This dissimilarity could be attributed to the datasets sharing patterns or structural features that are difficult to detect using the ANSE-method alone, and this method does not work for this pair class.

**4. *EST1Rn* vs. *EST2Rn* – Demolition Pattern Similarity pair class:**

- *ANN Similarity (Enhanced)*: 0.854478 (High Similarity);
- *Latest ANN method score*: **0.743335** (Moderate Similarity through Dissimilarity measures);

**Analysis:** Both methods actually indicate perfect similarity between *EST1Rn* and *EST2Rn* – datasets of negative changes in Tallin, fully aligning with the high similarity observed in both the statistical analysis [9], and in the ANN analysis for positive changes (see above). This confirms that the datasets are indeed highly similar, both structurally and in underlying patterns.

**5. *EST1Rn* vs. *KHNSRn* – War (Conflict) Zone Contrast pair class:**

- *ANN Similarity (Enhanced)*: 0.499366 (Low Similarity);
- *Latest ANN method score*: **0.329077** (Different Characteristics – Moderate Dissimilarity through Dissimilarity measures);

**Analysis:** The ANSE-score suggests low similarity, in contrast to the moderate dissimilarity from the latest method. This result might indicate that while the datasets differ in magnitude and simpler

metrics, because their demolished changes caused by urban redevelopment in one case, and by military hostilities in another one, they may share deeper, complex features detectable by both methods (Low Similarity; Moderate, but not High Dissimilarity).

**6. *EST2Rn* vs. *KHNSRn* – Demolition Type Differentiation pair class:**

- *ANN Similarity (Enhanced)*: 0.480926 (Low Similarity);
- *Latest ANN Method Score*: **0.424677** (Moderate to Low Dissimilarity through Dissimilarity measures)

**Analysis:** The score of 0.424677 from the second methods reflects moderate to low dissimilarity, generally consistent with the moderate similarity observed by the first method. This suggests that while there are some similarities between *EST2Rn* (demolished changes upon a normal urban redevelopment) and *KHNSRn* (demolished changes caused by military hostilities), they still exhibit notable differences, particularly in structural and complex patterns. It is necessary to mentioned that most significant differences among all pairs were expected exactly for this Sixth class according to the statistical analysis results [9], but it appeared not to be a case.

After the analysis provided, we should finalize the matter by comparing expected results for the nominal classes of pairs from the *Our research outline* subsection and the LANN-method results (Fig. 9), which align *partially* with the expected similarity/dissimilarity outcomes from prior research [9], with notable deviations in two cases:

**1. Aligned Expectations:**

- Classes 1–2 (*EST1n* vs. *EST2n*):
  - Score: **0.66** (Moderate Similarity);
  - Matches the expectation of *similar*.
- Classes 1–3 (*EST1n* vs. *KHNSn*):
  - Score: **0.60** (Moderate Similarity);
  - Consistent with the *similar* expectation.
- Classes 4–5 (*EST1Rn* vs. *EST2Rn*):
  - Score: **0.74** (Moderate Similarity);
  - Strong agreement with the *similar* expectation.
- Classes 4–6 (*EST1Rn* vs. *KHNSRn*):
  - Score: **0.32** (Different Characteristics);
  - Matches the *dissimilar* expectation.

**2. Deviations:**

- Classes 2–3 (*EST2n* vs. *KHNSn*):
  - Score: **0.35** (Different Characteristics);
  - Expected *slightly dissimilar*, but LANN indicates stronger dissimilarity.
- Classes 5–6 (*EST2Rn* vs. *KHNSRn*):
  - Score: **0.42** (Different Characteristics);
  - Expected *marginally dissimilar*, but LANN suggests intermediate dissimilarity.

**Implications:**

- The LANN method *overestimates dissimilarity* in classes 2–3 and 5–6 compared to statistical expectations (Fig. 9). This could reflect:
  - *Enhanced sensitivity* of the LANN to subtle feature differences (e.g., spatial or sequential patterns);
  - *Architectural bias* (e.g., deeper layers capturing non-linear relationships ignored by prior statistical models).
- Results for classes 1–2, 1–3, 4–5, and 4–6 validate the LANN's ability to replicate expected relationships.

Thus, the Latest ANN method successfully identifies core similarities/dissimilarities aligned with prior research but highlights additional granularity in dissimilar cases, potentially uncovering latent patterns missed by statistical analysis. Further investigation into the ANN feature representations (e.g., activation maps) could clarify these discrepancies.

**Conclusion.** Our study advances urban morphology analysis by integrating neural networks with LiDAR and GIS technologies to detect both routine urban redevelopments and disruptions caused by extraordinary events, such as armed hostilities. Focusing on Kharkiv, Ukraine - a city severely impacted by the 2022 Russian invasion - the research introduces two novel neural network methods: the *ANN Similarity (Enhanced)* (ANSE) and the *Latest ANN* (LANN). The ANSE method employs a feedforward architect-

ture with MSE loss and cosine similarity to predict similarity scores, while the LANN method utilizes deeper networks, contrastive loss, and Euclidean distance to emphasize dissimilarity, capturing nuanced spatial-temporal patterns.

Key findings reveal that the LANN method aligns with prior statistical expectations for most dataset pairs (e.g., routine redevelopment demolitions in Tallinn), demonstrating high accuracy in distinguishing similarity (scores 0.60–0.74). However, it overestimates dissimilarity in hostilities-related cases (e.g., Kharkiv war-induced demolitions), suggesting enhanced sensitivity to latent features like structural degradation or irregular redevelopment. These deviations highlight neural networks' capacity to uncover granular patterns overlooked by traditional models.

The framework's practical implications are quite significant: it may equip urban planners with scalable tools for monitoring post-war / post-disaster recovery, illegal encroachments, and ecological shifts. By automating 3D change detection, the methodology bridges gaps in conventional GIS-based approaches, offering actionable insights for equitable resource allocation and policy formulation. Future work should refine architectures (e.g., hybrid transformer-CNN models) and expand benchmark datasets to enhance generalizability. Ultimately, this research underscores AI's transformative role in fostering resilient, sustainable cities amid rapid urbanization and global crises.

### References

1. United Nations. (2018). *68% of the World Population Projected to live in Urban Areas by 2050, Says UN*. Department of Economic and Social Affairs. Available at: <https://www.un.org/development/desa/en/news/population/2018-revision-of-world-urbanization-prospects.html>
2. Weng O. (2012). Remote sensing of impervious surfaces in the urban areas: Requirements, methods, and trends. *Remote Sensing of Environment*. 117, 34-39. DOI: <https://doi.org/10.1016/j.rse.2011.02.030>.
3. Kostrikov S., Seryogin D. (2022). Urbogeosystemic Approach to Agglomeration Study within the Urban Remote Sensing Frameworks. *Urban Agglomeration*. Edited by A. Battisti and S. Baiani: Intech Open, London, Milan, Zagreb. 251-273. DOI: <http://dx.doi.org/10.5772/intechopen.102482>
4. Biljecki F., Stoter J., Ledoux H., Zlatanova S., Çöltekin A. (2015). Applications of 3D City Models: State of the Art Review. *ISPRS Int. J. Geo-Inf.* 4, 2842–2889. DOI: <https://doi.org/10.3390/ijgi4042842>
5. Kostrikov S., Niemets L., Sehida K. [and other]. (2018). Geoinformation approach to the urban geographic system research (case studies of Kharkiv region). *Visnyk of V.N. Karazin Kharkiv National University. Series "Geology. Geography. Ecology"*. (49), 107-121. DOI: <https://doi.org/10.26565/2410-7360-2018-49-09>
6. Kostrikov S., Kravchenko K., Serohin D., Bilianska S., Savchenko A. (2023). The performance of the digital city projects in urban studies of the megalopolises (the case studies of Kharkiv and Dnipro cities). *Visnyk of V. N. Karazin Kharkiv National University, series "Geology. Geography. Ecology"*, (59), 140-165. DOI: <https://doi.org/10.26565/2410-7360-2023-59-11>
7. Efe R., Onay T., Sharuno I., Atasoy E. (Editors.) (2014). *Urban and Urbanization*. Sofia: St. Kliment Ohridski University Press, 798.
8. Li Z., Chen B., Wu S., Su M., Chen J., Xu B. (2024). Deep learning for urban land use category classification: A review and experimental assessment. *Remote Sensing of Environment*. 311, 114290. DOI: <https://doi.org/10.1016/j.rse.2024.114290>
9. Kostrikov S., Niemets L., Robinson D., Mezentsev K., Kravchenko K., Serohin D. (2024). Delineation of the Hostilities' Impact on Urban Environment by LiDAR Data Processing (a Case Study of Kharkiv). In: Morar, C., Berman, L., Erdal, S., Niemets, L. (eds) *Achieving Sustainability in Ukraine through Military Brownfields Redevelopment*. NATOARW 2023. NATO Science for Peace and Security Series C: Environmental Security. Springer, Dordrecht. DOI: [https://doi.org/10.1007/978-94-024-2278-8\\_22](https://doi.org/10.1007/978-94-024-2278-8_22)
10. Gong P., Howarth P. J. (1992). Frequency-based contextual classification and gray-level vector reduction for land-use identification. *Photogrammetric Engineering and Remote Sensing*. 58(4), 423-437.



11. Gopal S., Woodcock C. E. (1996). Remote sensing of forest change using artificial neural networks. *IEEE Transactions on Geoscience and Remote Sensing*. 34(2), 398-404. DOI: <https://doi.org/10.1109/36.485117>.
12. Mas J. F. (1999). Monitoring land-cover changes: A comparison of change detection techniques. *International Journal of Remote Sensing*. 20(1), 139-152. DOI: <https://doi.org/10.1080/014311699213659>
13. Pijanowski B.C., Brown D.G., Shellito B.A., Manik G.A. (2002). Using neural networks and GIS to forecast land use changes: a Land Transformation Model. *Computers, Environment and Urban Systems*. 26 (6), 553-575. DOI: [https://doi.org/10.1016/S0198-9715\(01\)00015-1](https://doi.org/10.1016/S0198-9715(01)00015-1)
14. Yuan F., Sawaya K.E., Loeffelholz B.C., Bauer M.E. (2005). Land cover classification and change analysis of the Twin Cities (Minnesota) metropolitan area by multitemporal Landsat remote sensing. *Remote Sensing of Environment*. 98(2-3), 317-328. DOI: <https://doi.org/10.1016/j.rse.2005.08.006>
15. Lu, D., Mausel, P., Brondizio, E., Moran, E. (2004). Change detection techniques. *International Journal of Remote Sensing*. 25(12), 2365-2401. DOI: <https://doi.org/10.1080/0143116031000139863>
16. Li K., Hu X., Jiang H., Shu Z., Zhang M. (2020). Attention-Guided Multi-Scale Segmentation Neural Network for Interactive Extraction of Region Objects from High-Resolution Satellite Imagery. *Remote Sensing*, 12(5), 789. DOI: <https://doi.org/10.3390/rs12050789>
17. Daudt R., Saux B., Boulch A., Gousseau Y. (2018). Urban change detection for multispectral Earth observation using convolutional neural networks. *IGARSS 2018 - 2018 IEEE International Geoscience and Remote Sensing Symposium. IEEE Xplore*. DOI: <https://doi.org/10.1109/IGARSS.2018.8518015>
18. Chen J., Gong P., He C., Pu, R., Shi P. (2003). Land-use / land-cover change detection using improved change-vector analysis. *Photogrammetric Engineering & Remote Sensing*, 69(4), 369-379. DOI: <https://doi.org/10.14358/PERS.69.4.369>
19. Hussain M., Chen D., Cheng A., Wei H., Stanley D. (2013). Change detection from remotely sensed images: From pixel-based to object-based approaches. *ISPRS Journal of Photogrammetry and Remote Sensing*. 80, 91-106. DOI: <https://doi.org/10.1016/j.isprsjprs.2013.03.006>
20. Boulila W., Ghadorh H., Khan M., Ahmed F., Jawad Ahmad (2021). A novel CNN-LSTM-based approach to predict urban expansion. *Ecological Informatics*. 64, 101325. DOI: <https://doi.org/10.1016/j.ecoinf.2021.101325>
21. Zhu Z., Woodcock C. E. (2014). Continuous change detection and classification of land cover using all available Landsat data. *Remote Sensing of Environment*. 144, 152-171. DOI: <https://doi.org/10.1016/j.rse.2014.01.011>
22. Shi W., Zhang M., Zhang R., Chen S., Zhan Z. (2020). Change Detection Based on Artificial Intelligence: State-of-the-Art and Challenges. *Remote Sensing*, 12(10), 1688. DOI: <https://doi.org/10.3390/rs12101688>
23. You Y., Cao J., Zhou W. (2020). A Survey of Change Detection Methods Based on Remote Sensing Images for Multi-Source and Multi-Objective Scenarios. *Remote Sensing*. 12(15), 2460. DOI: <https://doi.org/10.3390/rs12152460>
24. Tian S., Ma A., Zheng Z., Zhong Y. (2020). Hi-UCD: A large-scale dataset for urban semantic change detection in remote sensing imagery. *arXiv preprint arXiv:2011.03247*. DOI: <https://doi.org/10.48550/arXiv.2011.03247>
25. Wang M., Tan K., Jia X., Wang X., Chen Y. (2020). A Deep Siamese Network with Hybrid Convolutional Feature Extraction Module for Change Detection Based on Multi-sensor Remote Sensing Images. *Remote Sensing*, 12(2), 205. DOI: <https://doi.org/10.3390/rs12020205>
26. Ankit U. (2024). Transformer Neural Networks: A Step-by-Step Breakdown [Electronic resource]. Built-In. Available at: [https://builtin.com/artificial-intelligence/transformer-neural-network?utm\\_source=chatgpt.com](https://builtin.com/artificial-intelligence/transformer-neural-network?utm_source=chatgpt.com)
27. Radke R.J., Andra S., Al-Kofahi O., Roysam B. (2005). Image change detection algorithms: a systematic survey. *IEEE Transactions on Image Processing*. 14(3), 294-307. DOI: <https://doi.org/10.1109/TIP.2004.838698>
28. Yan J., Wang L. Song W., Chen Y., Chen X., Deng Z. (2019). A time-series classification approach based on change detection for rapid land cover mapping. *ISPRS Journal of Photogrammetry and Remote Sensing*. 158, 249-262. DOI: <https://doi.org/10.1016/j.isprsjprs.2019.10.003>
29. Reba M., Seto K. C. (2020). A systematic review and assessment of algorithms to detect, characterize, and monitor urban land change. *Remote sensing of environment*, 242, 111739. DOI: <https://doi.org/10.1016/j.rse.2020.111739>
30. Zitzlsberger G., Podhorányi M., Svatoň V., Lazeký M., Martinovič J. (2021). Neural Network-Based Urban Change Monitoring with Deep-Temporal Multispectral and SAR Remote Sensing Data. *Remote Sensing*, 13(15), 3000. DOI: <https://doi.org/10.3390/rs13153000>
31. Hu F., Xia G.-S., Hu J., Zhang, L. (2015). Transferring Deep Convolutional Neural Networks for the Scene Classification of High-Resolution Remote Sensing Imagery. *Remote Sensing*. 7(11), 14680-14707. DOI: <https://doi.org/10.3390/rs71114680>
32. Jaiswal S. (2025). Multilayer perceptrons in machine learning: a comprehensive guide. DataCamp. 2025. Available online: [https://www.datacamp.com/tutorial/multilayer-perceptrons-in-machine-learning?utm\\_source=chatgpt.com](https://www.datacamp.com/tutorial/multilayer-perceptrons-in-machine-learning?utm_source=chatgpt.com)
33. Principe J.C., Euliano N.R., Lefebvre W.C. (1999). *Neural and Adaptive Systems: Fundamentals through Simulations*. New York: John Wiley & Sons. 656.
34. Jimenez-Lopez E, Lopez-Rivero L.A. (2023). Artificial neural networks in the application of the growth of the urban sprawl. *Publicacion Semestral Padi*. 11(21), 109-119. DOI: <http://dx.doi.org/10.29057/icbi.v11i21.10565>
35. Zygmunt M., Gawin D. (2021). Application of Artificial Neural Networks in the Urban Building Energy Modelling of Polish Residential Building Stock. *Energies*, 14(24), 8285. DOI: <https://doi.org/10.3390/en14248285>
36. Kuang Z., Su J., Latifian A., Eshraghi S., Ghafri A. (2024) Utilizing Artificial neural networks (ANN) to regulate Smart cities for sustainable Urban Development and Safeguarding Citizen rights. *Scientific Reports*. 14, 31592. DO: <https://doi.org/10.1038/s41598-024-76964-z>

37. Kostrikov S., Pudlo R., Bubnov D., Vasiliev V. (2020). ELiT, multifunctional web-software for feature extraction from 3D LiDAR point clouds. *ISPRS International Journal of Geo-Information*. 9(11), 650-885. DOI: <http://dx.doi.org/10.3390/ijgi9110650>
38. Wang J., Lindenbergh R., Menent, M. (2017). SigVox – A 3D feature matching algorithm for automatic street object recognition in mobile laser scanning point clouds. *ISPRS Journal of Photogrammetry & Remote Sensing*. 128, 111-129. <https://doi.org/10.1016/j.isprsjprs.2017.03.012>.
39. Wang Y., Chen Q., Liu L., Li X., Sangaiah A.K., Li K. (2018). Systematic Comparison of Power Line Classification Methods from ALS and MLS Point Cloud Data. *Remote Sens*. 10, 1222. DOI: <https://doi.org/10.3390/rs10081222>.
40. Cheng L., Wu Y., Tong L., Chen Y., Li M. (2015). Hierarchical registration method for airborne and vehicle LiDAR point cloud. *Remote Sensing* 7, 13921–13944. <https://doi.org/10.3390/rs71013921>.
41. Republic of Estonia. Land and Spatial Development Board (2025). Estonian Geoportal. Available at: <https://xgis.maaamet.ee/xgis2/page/app/maainfo>
42. Kleemann F., Lehner H., Szczypińska A., Lederer J., Fellner J. (2017). Using change detection data to assess amount and composition of demolition waste from buildings in Vienna. *Resource Conservation Recycling*. 123, 37-46. <https://doi.org/10.1016/j.resconrec.2016.06.010>
43. Zhan Y., Zhan Y., Fu K., Yan M., Sun X., Wang H., Qiu X. (2017). Change Detection Based on Deep Siamese Convolutional Network for Optical Aerial Images. *IEEE Geoscience and Remote Sensing Letters*. 14 (10), 1845-1849. DOI: <https://doi.org/10.1109/LGRS.2017.2738149>
44. Kashtan V., Hnatushenko V. (2024). Machine learning for automatic extraction of water bodies using Sentinel-2 imagery. *Radio Electronics, Computer Science, Control*. 1, 118-127. DOI: <https://doi.org/10.15588/1607-3274-2024-1-11>
45. LeCun Y., Bottou L., Bengio Y., Haffner P. (1998). Gradient-Based Learning Applied to Document Recognition. *Proceedings of the IEEE*, 86(11), 2278–2324. DOI: <https://doi.org/10.1109/5.726791>

## Аналіз змін міської морфології з використанням нейронних мереж

**Сергій Костріков**

д. геогр. н., професор, кафедра соціально-економічної географії  
та регіоналістики імені Костянтина Немця,

Харківський національний університет імені В.Н. Каразіна, Харків, Україна

Стаття висвітлює інтеграцію штучних нейронних мереж (ШНМ) із технологіями лідарного зондування та ГІС для аналізу змін у морфології урбанізованого середовища. Основна мета дослідження полягає в розробці та апробації відповідного підходу до кількісного та якісного оцінювання морфологічних змін як за умов рутинного міського розвитку, так і змін-порушень як наслідків війни. Доводиться, що класичні підходи недостатньо ефективні для виявлення протилежних за динамікою просторово-часових змін. Сучасні методи на базі глибокого навчання дозволяють не тільки аналізувати лідарні хмари точок, але й ефективно впроваджувати компаративний аналіз наборів даних щодо різних локацій міста. Нами було розроблено два методи нейромережевого аналізу:

1. *ANSE-метод*: використовує багаторівневу мережу з функцією втрат MSE (середньоквадратична помилка) та косинусною мірою схожості для порівняння наборів даних.
2. *LANN-метод*: застосовує глибоку архітектуру з контрастивною функцією втрат та евклідовою відстанню, що акцентує увагу на відмінностях, зокрема для виявлення аномалій (наприклад, руйнувань від обстрілів).

Авторське програмне забезпечення *iQ City Change Management* застосовувалося для обробки лідарних даних по двох часових реперах з різницею у три (Харків) й п'ять (Таллінн) років. Виконувалося виокремлення моделей будівель й класифікація морфологічних змін. Для Харкова проаналізовано 4 км<sup>2</sup> району Північна Салтівка: виявлено 215 «додатних» об'єктів (зміни у 2019-2021) та 51 «від'ємних» (руйнування навесні 2022). Контрольне порівняння з Таллінном (Естонія, зміни у 2017-2022) підтвердили прийнятну точність методів для рутинних змін у міському доквіллі (ШНМ-оцінка схожості 0.60-0,66 додатних змін між Харковом та Таллінном; 0,74 – від'ємних змін між двома локаціями у Таллінні).

*Ключові результати:*

- LANN-метод виявив суттєві відмінності між змінами під час війни й у мирний час (наприклад, ШНМ-оцінка схожості 0,35 та 0,32-0,42 для порівняння додатних та від'ємних змін між Харковом та Таллінном), що вказує на чутливість до структурних аномалій (наприклад, хаотичний розподіл руйнацій у порівнянні з «запланованими від'ємними» змінами).
- ANSE-метод ефективний для стандартних задач мирного часу, але недооцінює складність подання воєнних руйнувань.

*Практичне значення:* запропонований підхід надає інструменти для моніторингу відбудови міст, оптимізації ресурсів та аналізу морфологічних змін. Інтеграція ШНМ із лідарними даними розширює можливості ГІС, особливо в умовах обмеженої кількості джерел даних.

**Ключові слова:** ЛІДАР, міські дослідження, дистанційне міське зондування, ГІС-додаток, виокремлення забудов, визначення змін, нейронні мережі, аналітичне програмне забезпечення, нейромережеві аналітичні методи.

Надійшла 17 лютого 2025 р.

Прийнята 23 квітня 2025 р.